El-Hussain *et al. Geosci. Lett.* (2018) 5:30
https://doi.org/10.1186/s40562-018-0129-4

Geoscience Letters

RESEARCH LETTER

Open Access

Probabilistic and deterministic estimates of near-field tsunami hazards in northeast Oman

I. El-Hussain[1*], R. Omira[2,3], Z. Al-Habsi[1], M. A. Baptista[3,4], A. Deif[1] and A. M. E. Mohamed[1]

Abstract

Tsunamis generated along the Makran subduction zone (MSZ) threaten the Sur coast of Oman, according to deterministic and probabilistic analyses presented here. A validated shallow water numerical code simulates the source-to-coast propagation and quantifies the coastal hazard in terms of maximum water level, flow depth, and inundation distance. The worst-case source assumed for the eastern MSZ is a thrust earthquake of Mw 8.8. This deterministic scenario produces simulated wave heights reaching 2.5 m on the Sur coast leading to limited coastal inundation extent. Because Oman adjoins the western MSZ, the probabilistic analysis includes the effect of this segment also. The probabilistic analysis shows onshore inundations exceeding 0.4 km northwest of Sur where flow depths are likely to exceed 1 m in 500 years. Probability analysis shows lesser inundation areas with probability of exceeding 1 m flow depth up to 80% in 500-year exposure time. Teletsunamis are excluded from these analyses because far-field waves of the 2004 Indian Ocean tsunami did not impact the Sur coast. Also excluded for simplicity are tsunamis generated by submarine slides within or near MSZ rupture areas. The results of this research provide essential information for coastal planning, engineering and management in terms of tsunami hazard and an essential step toward tsunami risk reductions in the northwest Indian Ocean.

Keywords: Tsunami, Oman Sea, Oman, Deterministic and probabilistic methods

Introduction

In the aftermath of the 2004 Indian Ocean tsunami, tsunami science gained particular attention from the scientific community, stakeholders, and humanitarian organizations, all with the objective to protect the endangered coastal population and to mitigate the tsunami impact from future events. Seven years later, the 2011 Tohoku tsunami raised serious questions about tsunami disaster countermeasures, the coastal effects of tsunami and the need to quantify the tsunami hazard (Mori et al. 2011). Both deterministic and probabilistic hazard assessment models are utilized to better serve planners for developing tsunami mitigation measures.

Deterministic and probabilistic approaches reached commonly accepted formulations in use for assessing the tsunami hazard in various coastal zones around the world. The deterministic, also called scenario-based, approach uses a particular source scenario (maximum credible or worst-case scenario) to calculate the ensuing tsunami impact at the coastal areas of interest (Tinti and Armigliato 2003; Tinti et al. 2005; Løvholt et al. 2006; Lorito et al. 2008; Harbitz et al. 2012; Omira et al. 2013). The products of this method consist of maps depicting the wave height, the coastal inundation and the flow velocity. The probabilistic approach, on the other hand, estimates the likelihood of tsunami impact taking into consideration a broad range of near- and far-field potential sources as well as a treatment of the uncertainties on the hazard assessment (Geist and Parsons 2006). Probabilistic analysis involves full hazard curves at each coastal point of interest, from which the probability exceedance maps can be derived for any tsunami hazard metric (wave

*Correspondence: elhussain@squ.edu.om
[1] Earthquake Monitoring Center, Sultan Qaboos University (SQU), Muscat, Oman
Full list of author information is available at the end of the article

height, inundation depth, current speed, etc.) (Geist and Lynett 2014; Grezio et al. 2017).

Along the coast of Oman, tsunamis present a serious source of threat. The Omani coast was subjected to at least two confirmed tsunamis during the twentieth and twenty-first centuries: the 1945 tsunami due to an earthquake in the Makran subduction zone (MSZ) in the Arabian Sea (near-field tsunami) and the Indian Ocean tsunami in 2004, due to an earthquake from the Andaman Sumatra subduction zone (far-field tsunami). The impact of the 1945 tsunami was large in the Arabian Sea. It affected the Makran coast and the Indus Delta, the western coast of India, Iran and Oman, killing hundreds of people and causing great destruction (El-Hussain et al. 2016). Wave heights up to 15 m were estimated in Pasni and Ormara, now part of Pakistan. These tsunami wave heights have been difficult to explain solely by a tectonic seismic source, and submarine slides have been simulated as sources of the large waves at Pasni and Ormara (Rastgoftar and Soltanpour 2016; Heidarzadeh and Satake 2017). Moreover, the tsunami was reported in Sur and Muscat but no damage details are documented (Kakar et al. 2014, 2015; Hoffmann et al. 2013). The MSZ, where the 1945 tsunami was generated, is an active tectonic feature, about 900-km-long north-dipping thrust, where the Arabian plate subducts underneath the Iranian and Pakistani parts of the Eurasian plate (Fig. 1a).

In this paper, both deterministic and probabilistic methods are used to assess the tsunami hazard at Sur coastal, on the northern Omani coast. The MSZ is considered the main tectonic source zone. The impact of the Indian Ocean 2004 Sumatra tsunami was less severe, affecting only the southern coasts of Oman, and it did not reach the study area; therefore, this far tsunamigenic source is excluded from this study. Also, submarine landslides as well as mud-volcanos triggered by large earthquakes are excluded from this study for simplicity. Numerical modelling is used to simulate the tsunami propagation and inundation on a high-resolution digital elevation model of the target coast. Results are presented in terms of tsunami hazard maps depicting the maximum wave height and flow depth distributions (deterministic assessment) and 100- and 500-year probabilities of exceedance (probabilistic assessment) for the Sur coastal segment.

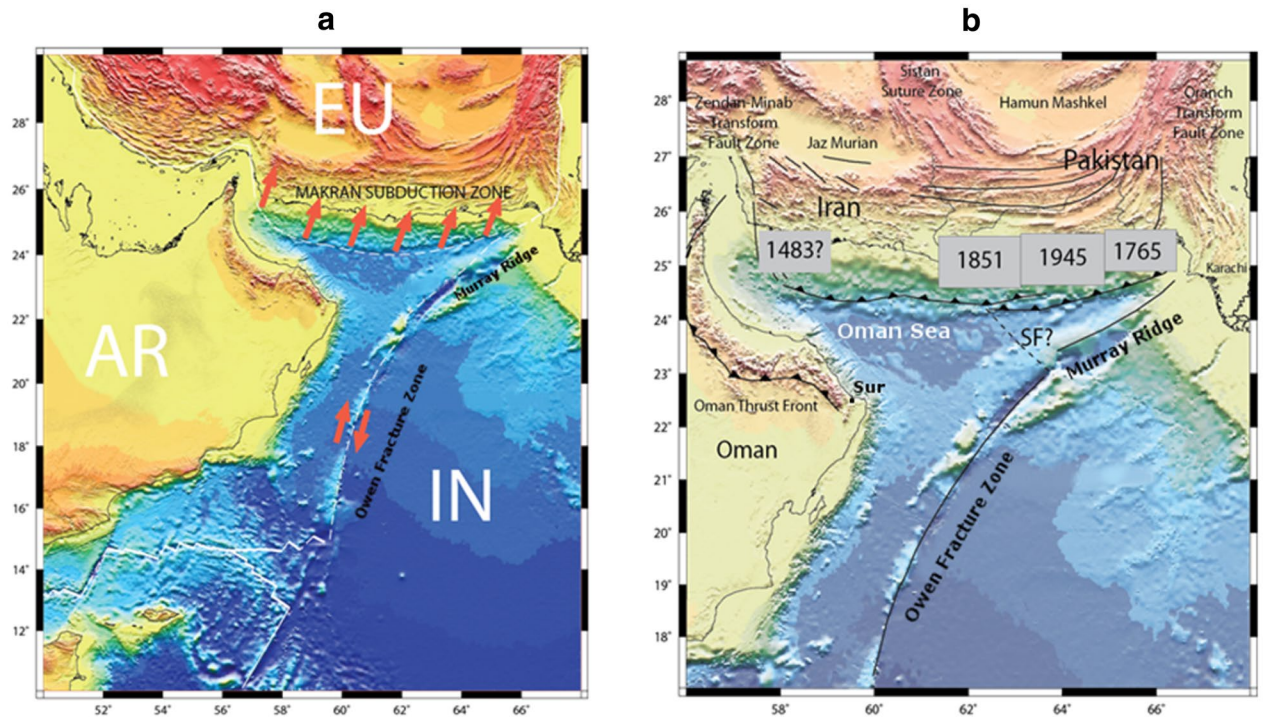

Fig. 1 **a** The tectonic framework of the Sea of Oman is constrained by the relative motion between the Arabian, Eurasian and India plates. The Arabian plate subducts underneath the Eurasian plate at a rate close to 2 cm/year while the relative motion between India and Arabia along the Owen strike slip boundary reaches 3.7 mm/year. **b** Ruptured area of strong earthquakes in Makran based on Byrne et al. (1992) and Zarifi (2006). SF: Sonne Fault, defining a small microplate, called Ormara microplate by Kukowski et al. (2000)

Tsunami sources

Near-field tsunamis

In this paper, the focus is on the Makran subduction zone (MSZ) (Fig. 1a) as the most important seismogenic zone able to cause tsunamis that might affect the coast of Oman. Within the MSZ, there is very dissimilar seismic activity, degree of deformation, as well as various rupture histories between the eastern and western zones (Minshull et al. 1992; Byrne et al. 1992). The segmentation of the MSZ in the western and eastern zones is geologically supported by the displacements in the Quaternary Calc-Alkaline volcanoes, topographic depression (Mashkal and Jaz Murian), and by the presence of two block structures of the overriding plate (Lut and Helmand, Fig. 1b). The borderline between these large-scale structures is approximately coincident with the transition in seismic activity between the eastern and western parts of MSZ (El-Hussain et al. 2017).

The seismicity of the Makran subduction zone is low and shows significant variation between its eastern and western segments. The eastern Makran (see Fig. 1a) has been ruptured throughout history by large earthquakes and currently is experiencing very low seismic activity in its fore-arc setting. McCall (2002) attributed the overall low seismicity of the Makran zone to the suggestion that the subduction is largely spent in slow movement, and that subduction is now relatively insignificant compared with crustal shortening in the Zagros orogenic belt. The difference in convergence would be accommodated by the Zendan Fault (Regard et al. 2010). There is some uncertainty regarding the rate of subduction in the MSZ. Vernant et al. (2004) estimate a value in the range of 19.5 ± 2 mm/year. GPS evidence shows significant differential movement between Oman and Iran with shortening of 19.5 mm/year, suggesting that subduction is taking place (Masson et al. 2007).

The historical record places seven large earthquakes in Makran since 1483. An event in 1765 was felt strongly in easternmost Makran (see Fig. 1b). Two coastal events occurred in 1851 and 1864 affecting the town of Gwadar (Quittmeyer and Jacob 1979), again in eastern Makran. Another large event occurred in 1914 in northern Makran (Gutenberg and Richter 1954). Gutenberg and Richter reported that this event occurred at a depth of 60–100 km, indicating that it was within the downgoing plate. On 27 November 1945, a great earthquake of Mw = 8.1 struck the coast of eastern Makran, followed by a large aftershock in 1947 immediately to the south.

The most notable earthquake is the November 27th, 1945, Gwadar earthquake (Mw = 8.1), a tsunamigenic event that killed about 300 deaths according to Ambraseys and Melville (1982). This earthquake is an inter-plate thrust event that produced a slip of 6.6 m (Byrne et al. 1992). The source parameters of the 1945 earthquake calculated by Byrne et al. (1992) are presented in Table 1. They believed that similar events would be expected to repeat at least every 175 years in eastern Makran. Page et al. (1979) estimated that the recurrence of a similar 1945-type earthquake along the MSZ is approximately 125–250 years. Quittmeyer and Jacob (1979) reported the intensity (in modified Mercalli scale), surface magnitude (Ms), and rupture length of the 1945 event to be 10, 8, and 150–200 km, respectively. The distribution of intensities and the long-term aftershock activity suggest that the rupture propagated to the east of the epicentre (Quittmeyer and Jacob 1979; Byrne et al. 1992).

Far-field tsunamis

The study considers only the tsunami impact from the MSZ "near-field" tectonic scenario as the far-field tectonic scenario from Indian Ocean generates modest tsunamis along the Omani coast. Assessment of the potential tsunami impact from a far-field tectonic scenario, namely the Indian Ocean tsunami of 26 December 2004, confirms the conclusions that tsunamis generated along the Andaman Sumatra subduction zone generate only modest tsunamis along the Arabian Sea and along the Omani coast (Okal et al. 2006; Burbidge et al. 2009). Moreover, the field survey results presented in Okal et al. (2006) show that tsunami wave heights from this far-field source area decrease towards the northeast coast

Table 1 Fault parameters of the deterministic scenarios

Scenario	Mw	Location[c]		Length (km)	Width (km)	Slip (m)	Dip (°)	Rake (°)	Strike (°)
		Latitude (°N)	Longitude (°E)						
EMSZ[a]	8.8	24.66	65.50	461	110	11	7	90	263
HMSZ[b]	8.1	24.55	64.36	150	70	6.6	7	90	261

[a] The Eastern Makran subduction zone scenario

[b] The historical Makran subduction zone earthquake of 27 November 1945

[c] The southeast corner of the fault plane

of Oman, with low wave height to be measurable in this study area.

Methods and data

Deterministic tsunami hazard assessment

The DTHA is the commonly used method to evaluate the hazard posed by tsunamis and has been applied by a number of scientific groups in various tsunami-prone coastal zones (Tinti and Armigliato 2003; Baptista et al. 2011; Omira et al. 2013). Some authors argue that DTHA can better serve the purpose of coastal engineering to develop tsunami mitigation measures as it allows deriving the maximum tsunami metrics (wave height, inundation extent, and depth) for the worst scenario, avoiding the complications associated with probabilistic analysis, which requires long return periods to assess such maximum tsunami impact characteristics. On the other hand, there is no single accepted way of defining the known worst scenario. Therefore, the accuracy of the DTHA results mainly relies on such a definition.

In general, the DTHA involves a number of steps that include (i) definition of the tsunami source area; (ii) characterisation and parameterization of the worst-case sources; (iii) modelling the tsunami generation; (iv) modelling the tsunami propagation in the deep ocean; and (v) simulation of the coastal inundation. These steps are used to produce the tsunami hazard maps, in terms of maximum wave height and inundation depth, for the target coast of Sur, Oman.

Our definition of the credible worst-case tsunami scenario for Sur-Oman coast is based on available seismic information that leads to a Mw 8.8 earthquake corresponding to the rupture of the total segment of the eastern MSZ. Other researchers postulated worst-case scenario with higher magnitudes and longer rupture length (Smith et al. 2013; Okal and Synolakis 2008; Heidarzadeh et al. 2009; Rashidi et al. 2018). Additionally, the event of November 27th, 1945, is considered due to its historical importance and the tsunami impact in the region. The earthquake fault parameters of these scenarios required for the modelling of the tsunami generation are depicted in Table 1.

Probabilistic tsunami hazard assessment

The PTHA approach has, in comparison to the DTHA, the advantage of including the contribution of possible small and large events and of treating different sources of uncertainty in tsunami hazard assessment. Therefore, it is seen as a more complete approach for evaluating the hazard posed by tsunamis.

Here, only the tsunamis induced by earthquake sources are considered in the MSZ and to find the probability that a wave height/flow depth exceeds a certain level following the occurrence of possible tsunami events. To do this, the logic-tree framework developed by El-Hussain et al. (2016) and Omira et al. (2016a) is used incorporating the following nodes: (i) definition of the tsunamigenic source zones within the MSZ; (ii) generation of the earthquake scenario database within each source zone (individual magnitudes and fault parameters); (iii) deriving the earthquake recurrence rate; (iv) numerical simulation of the tsunami, associated with each defined scenario, from the source to the target coast; and (v) deriving the tsunami probability of exceedance using statistical methods. A detailed description of the different nodes of the logic-tree is depicted in Fig. 2. The "node 0" of the logic-tree corresponds to the occurrence of an earthquake event (E) within the near-field (MSZ) or the far-filed source region. As our study only focusses on the near-filed source region, the probabilistic calculation is started from the

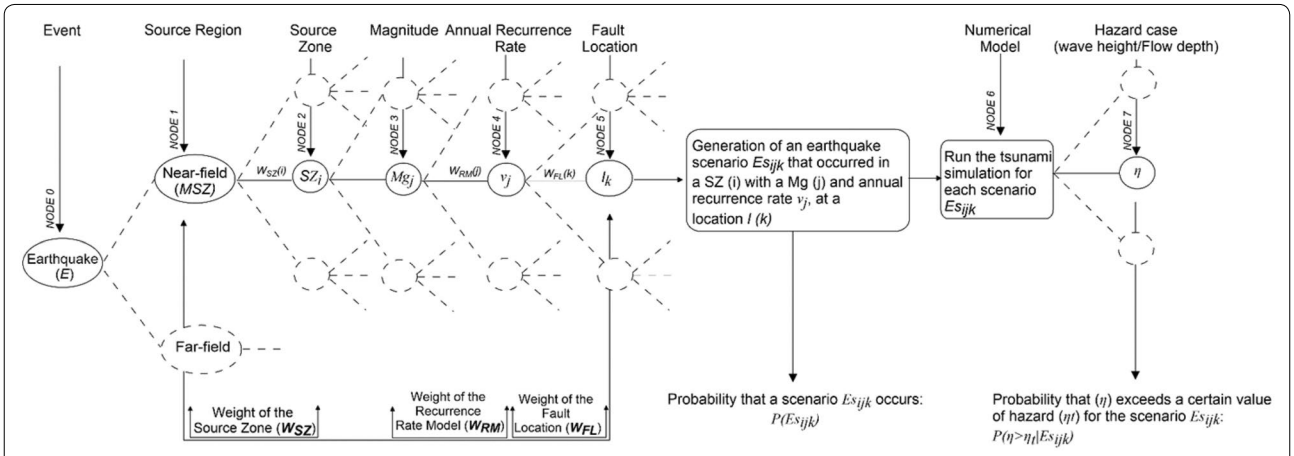

Fig. 2 Logic tree developed for probabilistic tsunami hazard assessment along the coast of Oman

"node 1" with the selection of the MSZ as a source region (Fig. 2).

To establish, for multiple sources, the joint probability that a wave height/flow depth exceeds a particular value for a given exposure time, the sources are considered independent (as in the Poisson distribution). This process allows for the calculation of the time-independent probability that wave height/flow depth will be exceeded due to the occurrence of an earthquake scenario (Omira et al. 2015, 2016a). A detailed description of the PTHA framework used in this study can be found in previous works (Omira et al. 2015, 2016a; El-Hussain et al. 2016).

Since the PTHA requires considering the contribution of large and small events, a database is generated with the probabilistic tsunami scenarios. This process involves the following steps: (i) identify the tsunamigenic source zones; (ii) define the magnitude interval for each source zone; (iii) determine the recurrence rate of each individual magnitude; (iv) associate a typical fault (TF) for each individual magnitude; (v) let the TF float along the fault trace.

Within the MSZ, two source zones are considered, namely the eastern Makran source zone (EMSZ) and the western Makran source zone (WMSZ). The PTHA tsunamigenic scenarios include earthquake magnitudes ranging from Mw 7.5 to the Mw of the worst-case scenario with a regular interval of 0.2 between individual magnitudes. The recurrence rate of each individual magnitude is calculated using two different seismic probability models, Molnar (1979) and Deif and El Hussain (2012), based on moment rate. TFs are then defined through establishing the dimensions of the fault (length, width, and depth), the strike, rake and dip angles of the earthquake rupture. These parameters are used to compute the sea bottom deformation needed to initiate the tsunami simulation. The PTHA scenario database proposed by El-Hussain et al. (2016) is used to evaluate probabilistic tsunami hazard along the entire Omani coast from the earthquake events generated within the MSZ.

It is worth pointing out that the mix of the DTHA and PTHA presented here reflects today's limited understanding of MSZ earthquake history and potential. The large variation in the seismicity pattern between the eastern and western parts of MSZ, along with the variation of rupture histories (Minshull et al. 1992; Musson 2009) and many geological observations led to the postulation that the eastern part is entirely separate from the western Makran. This provides a good explanation of why most of the seismic activity occurs in the eastern part of the zone, and the western part is quiet. Therefore, a single event rupturing both parts of the Makran together is improbable. The dimensions of each part make the occurrence of earthquakes of order of Mw 9.0 or greater unlikely. Previous studies appear to have ruled out the possibility of aseismic subduction and postulated that the fault is locked without conclusive evidences in hand (Smith et al. 2013; Okal and Synolakis 2008; Heidarzadeh et al. 2009; Rashidi et al. 2018). Bayer et al. (2006) argued that the absence of large earthquakes in the western Makran can be explained by the presence of a great amount of unconsolidated and water saturated weak sediments lubricating relative plate movement to constrain seismicity. Additionally, Pararas-Carayannis (2006) indicated that the western part of MSZ shows much more fracturing, indicating that earthquakes would be expected to be smaller magnitude events (less than 7) and to have shorter ruptures (less than 100 km) along sub-segments. Therefore, the worst-case scenario in this study is limited to the present knowledge of the geophysical problem and area, and the probabilistic analysis is restricted to the MSZ.

Tsunami simulation setup

To generate the initial conditions of the tsunami propagation model, the co-seismic deformation due to the submarine earthquake is computed. Okada's (1985) half-space elastic equations are used to compute the sea bottom deformation due to the earthquake assuming that the water is an incompressible fluid and the initial sea surface elevation mimics the sea bottom deformation. The initial sea surface elevation and the zero velocity constitute the initial conditions of the simulation model.

Once the initial tsunami conditions are calculated, a non-linear shallow water model (NSWING—non-linear shallow water with nested grids) is used to simulate the tsunami propagation from the source zone towards the coast, including inundation. NSWING was benchmarked (Miranda et al. 2014) and used to simulate recent tsunami events (Omira et al. 2016b). The code employs a dynamically coupled system of nested grids and solves, in spherical or Cartesian coordinates, the shallow water equations using an explicit staggered leap-frog finite differences scheme for linear terms and an upwind scheme for the non-linear terms in both. An open boundary condition is used on the outward limit of the grid, whenever it does not correspond to land. To simulate the tsunami inundation, the moving boundary treatment (Liu et al. 1995), based upon "wet" and "dry" cells, is adopted to properly track shoreline movements. The NSWING code is entirely written in C, with an easy-to-use interface following the GMT (Wessel et al. 2013) style and core parallelisation to faster computing performance and to allow for its use in more computing intensive problems. It also handles generic file formats (e.g. netCDF) and produces outputs that correspond to the basic needs of scientific users: synthetic tsunami waveforms, time snapshots of

water elevation or velocity components, tsunami inundation and energy patterns.

Digital elevation model

The simulation of the tsunami propagation and coastal inundation critically depends on the quality of data used in addition to the capability of the numerical model to accurately simulate the different phases of the tsunami life. Therefore, the coastal DEM (digital elevation model) must be able to accurately represent the most significant bathymetric and topographic features and the shoreline.

In this work, a set of digital elevation models (DEMs) is generated with increasing resolution from the source area towards the target coast (Fig. 3). These DEMs were produced including (i) the tsunami source area and the coastal areas of interest; (ii) good horizontal resolution in the test areas to assure a full description of local effects; and (iii) continuity offshore–onshore, in particular, in respect to the vertical datum.

To build the different digital elevation models, a compilation of multisource elevation/depth data was considered. This includes data from GEBCO with 30-s arc resolution (https://www.gebco.net); the nautical charts (scales: 1:15,000 and 1:30,000 and IDs: OM_3518_5 and OM_3518_6); 30-m resolution topography data from ASTER Global Digital Elevation Model (ASTER GDEM, http://www.jspacesystems.or.jp/ersdac/GDEM/E/index.html); and near-shore bathymetric and topographic charts (n°: SIPM Co.1994) with projection PSD93 (datum of Clarke 1880 ellipsoid).

To ensure accurate simulation of near-shore tsunami propagation and coastal inundation, the constructed DEMs were nested in a system of two grids of increasing resolutions: 1200 m and 100 m (Fig. 3). The 1200-m grid was built from the 30-s arc GEBCO data, while the 100-m grid resulted from a compilation of ASTER data, nautical charts, and near-shore elevation charts. The finer grid (GRID 2 in Fig. 3b) focuses on the coastal area of Sur, Oman.

The tsunami simulations ran for 8 h of propagation to ensure that the target coasts are reached. A 1-s time step is used in the coarse grid, to guarantee the CFL numerical stability condition.

Results and discussion

DTHA results

The DTHA results are presented for the Mw 8.8 worst-case and the 1945-like scenarios in terms of regional and local hazard maps. The regional hazard maps depict the large-scale source-to-coast tsunami propagation. The hazard is expressed in terms of maximum wave height and tsunami travel time. The local hazard maps depict the high-resolution near-shore maximum wave height and the inundation hazard. Inundation is described in terms of flow depth. Figures 4 and 5 depict the DTHA results for both worst-case and 1945-like scenarios, respectively.

For the Mw 8.8 worst-case tsunami scenario, the results presented in Fig. 4a show that the rupture of 461 km along the eastern MSZ radiates most of the tsunami energy to the coast of Pakistan and to the southeast Indian Ocean. The dislocation along the fault plane, exceeding 10 m, generates maximum wave heights that can reach 8 m along the coast of Pakistan. Offshore of the Omani coast, tsunami wave heights are in the range of 0.5–2 m. The tsunami travel time simulation depicted in Fig. 4a shows that the first wave reaches the Sur coast in approximately 25 min after the earthquake occurrence. The fact that most of the energy is steered away from Oman does not preclude the existence of significant effects in the shallow water areas of the Omani coast. This is clearly noticeable along the Sur coast in high-resolution simulations (Fig. 4b), where the wave heights range from 1 to 2 m and reach 2.5 m at some locations. This leads to flooding of some low-lying coastal areas in Sur with flow depths varying from few centimetres to about 1 m (Fig. 4b).

For the 1945-like scenario, examination of the results indicates that most tsunami energy is steered toward the coast of Pakistan and toward the southeast of the Arabian Sea with maximum wave amplitude of about 2 m. Along the coast of Oman, the tsunami hazard is low in terms of maximum wave height distribution (Fig. 5a). The first wave reaches the coast of Oman in less than 1 h (approximately about 50 min; Fig. 5a). Maximum wave heights in the area of interest (Sur coast) are less than 0.5 m (Fig. 5a), whereas the high-resolution simulations show that the incident waves undergo shoaling effects in shallow water areas leading to increase their amplitudes that reach 1.4 m at some locations (Fig. 5b). As a consequence, tsunami inundation is limited to some few coastal locations of low topographic elevations (Fig. 5b). Therefore, the occurrence of a similar event today does not pose a major threat to the coast of Oman. However, it should be mentioned that, in case of occurrence of such an earthquake, all low beach areas must be evacuated.

PTHA results

PTHA concerns only the tsunamis generated in the MSZ. PTHA results are presented in terms of maps depicting the probability that a tsunami maximum wave height/flow depth exceeds 0, 0.5, 1.0, and 1.5 m in 100- and 500-year exposure times.

Figure 6 depicts the 100-year exposure time probability that a maximum wave height offshore and a flow depth onshore exceed 0 m (Fig. 6a), 0.5 m (Fig. 6b), 1 m (Fig. 6c), and 1.5 m (Fig. 6d) along the coastal segment

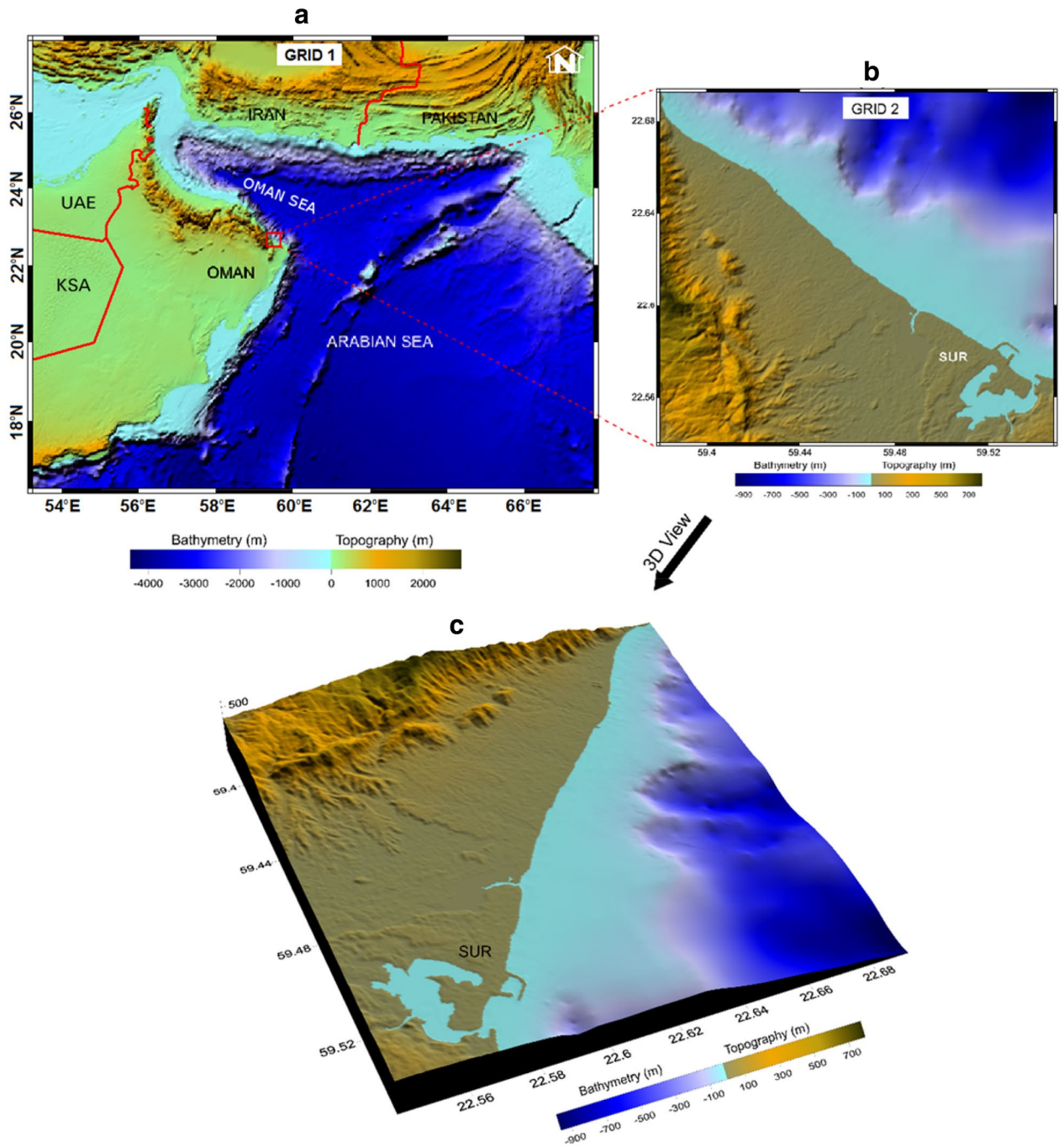

Fig. 3 Digital elevation models: **a** regional bathymetric/topographic model with 1200-m horizontal resolution, **b** high-resolution (100 m) DEM of the Sur coast and **c** 3D view of the high-resolution DEM

of Sur, Oman. The 100-year PTHA maps clearly show a moderate tsunami hazard along the study coast from the MSZ earthquakes. As expected, this hazard decreases with the increase of the tsunami intensity threshold (maximum wave height or flow depth). For 100-year average return time, the probability that a maximum wave height exceeds 0.5 m reaches 100% along the entire target coast (Fig. 6b). This probability ranges from 50 to 80% and from 20 to 60% for maximum wave height thresholds of 1 m and 1.5 m,

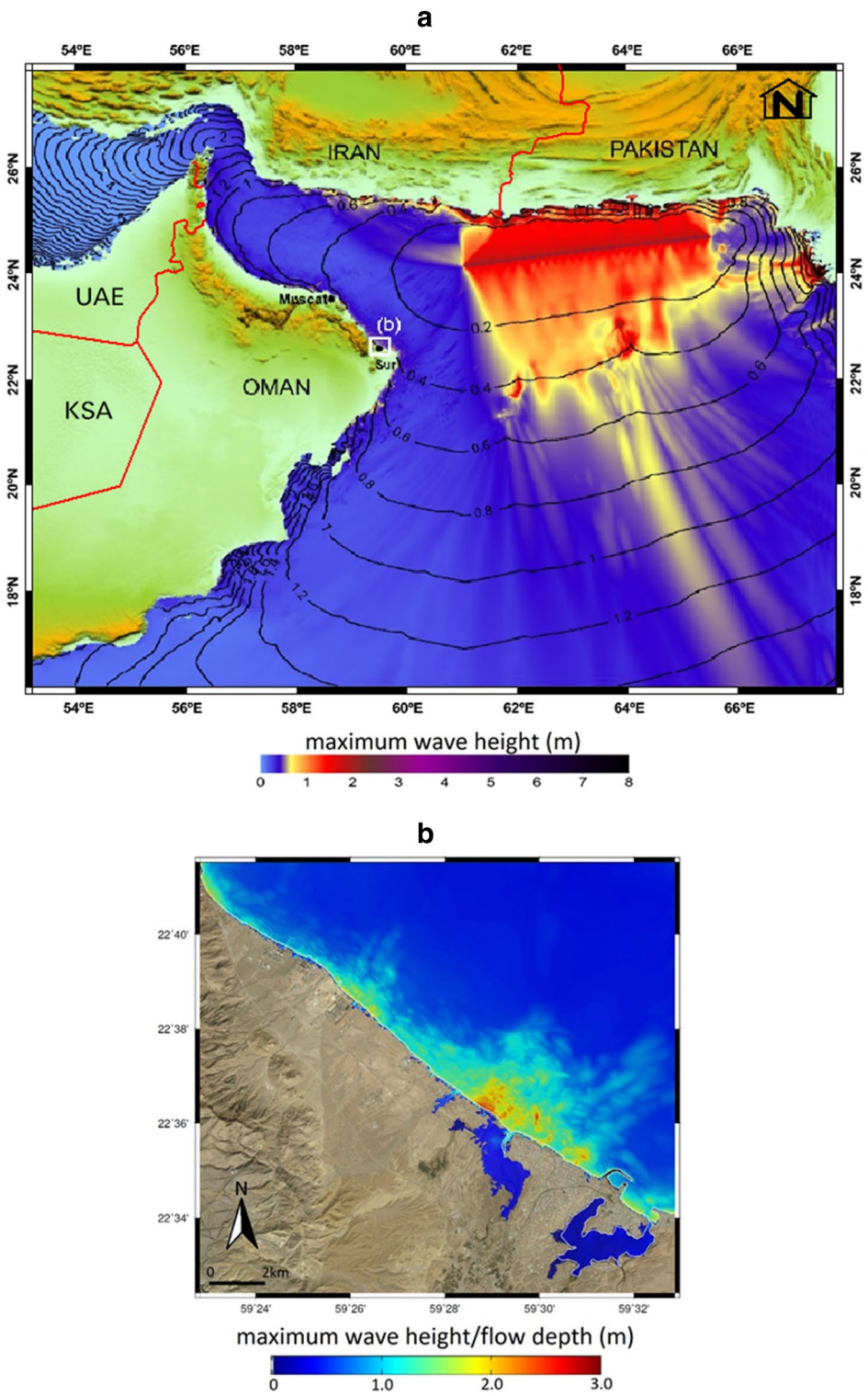

Fig. 4 **a** Maximum wave height distribution in the Arabian Sea following the occurrence of a Mw 8.8 earthquake event in the eastern segment of the MSZ. The contours represent the tsunami travel time in hours and plotted every 0.2 h; **b** maximum wave height and maximum flow depth distribution along the coastal segment Sur due to the occurrence of a Mw 8.8 earthquake event

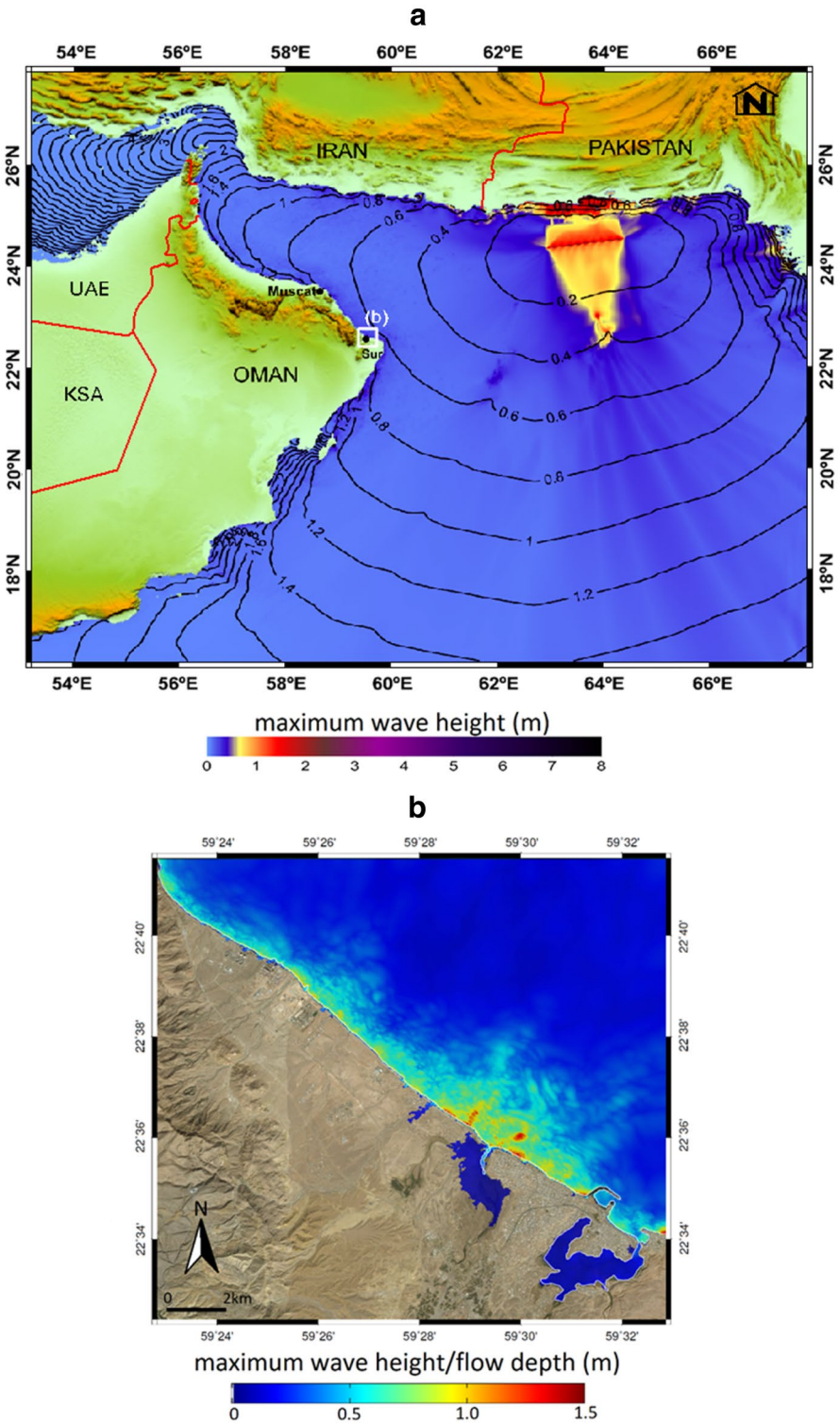

Fig. 5 **a** Maximum wave height distribution in the Arabian Sea following the occurrence of a Mw 8.1 1945-like earthquake event in the eastern MSZ. The contours represent the tsunami travel time in hours plotted every 0.2 h, **b** maximum wave height and maximum flow depth distribution along the coastal segment Sur due to the occurrence of a 1945-like event

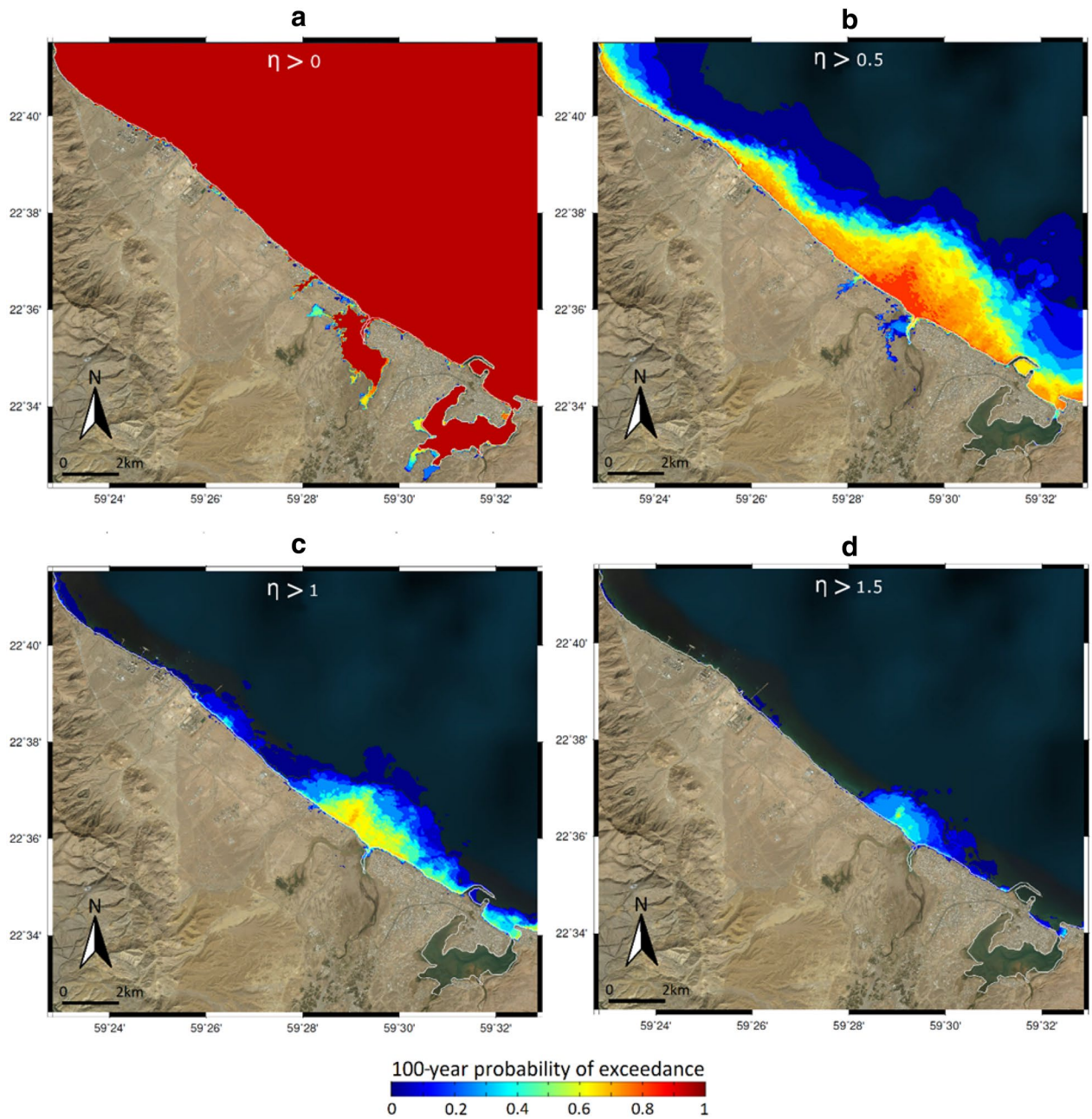

Fig. 6 Probability that the maximum wave height/flow depth **a** exceeds 0 m, **b** exceeds 0.5 m, **c** exceeds 1 m, and **d** exceeds 1.5 m along the coastal segment of Sur, Oman, for an exposure time of 100 years. η = wave height–flow depth threshold. The scale bar unit is the probability from 0 to 100% (0.8 = 80%)

respectively (Fig. 6c, d). Onshore, the probability of inundation occurrence (flow depth >0 m, Fig. 6a) is about 100% at some specific low-lying coastal areas. A significant decrease of the flood probability is noticeable in the following situations: when moving towards higher coastal zones and when considering larger values of the flow depth threshold (Fig. 6b–d).

Figure 7 shows, for an exposure time of 500 years, the probability that a maximum wave height/flow depth exceeds 0 m (Fig. 7a), 0.5 m (Fig. 7b), 1 m (Fig. 7c), and 1.5 m (Fig. 7d) along the coastal segment of Sur, Oman. The probability maps highlight a high level of tsunami hazard in 500-year exposure time as the probability of exceeding 1.5 m wave height reaches 100% at some

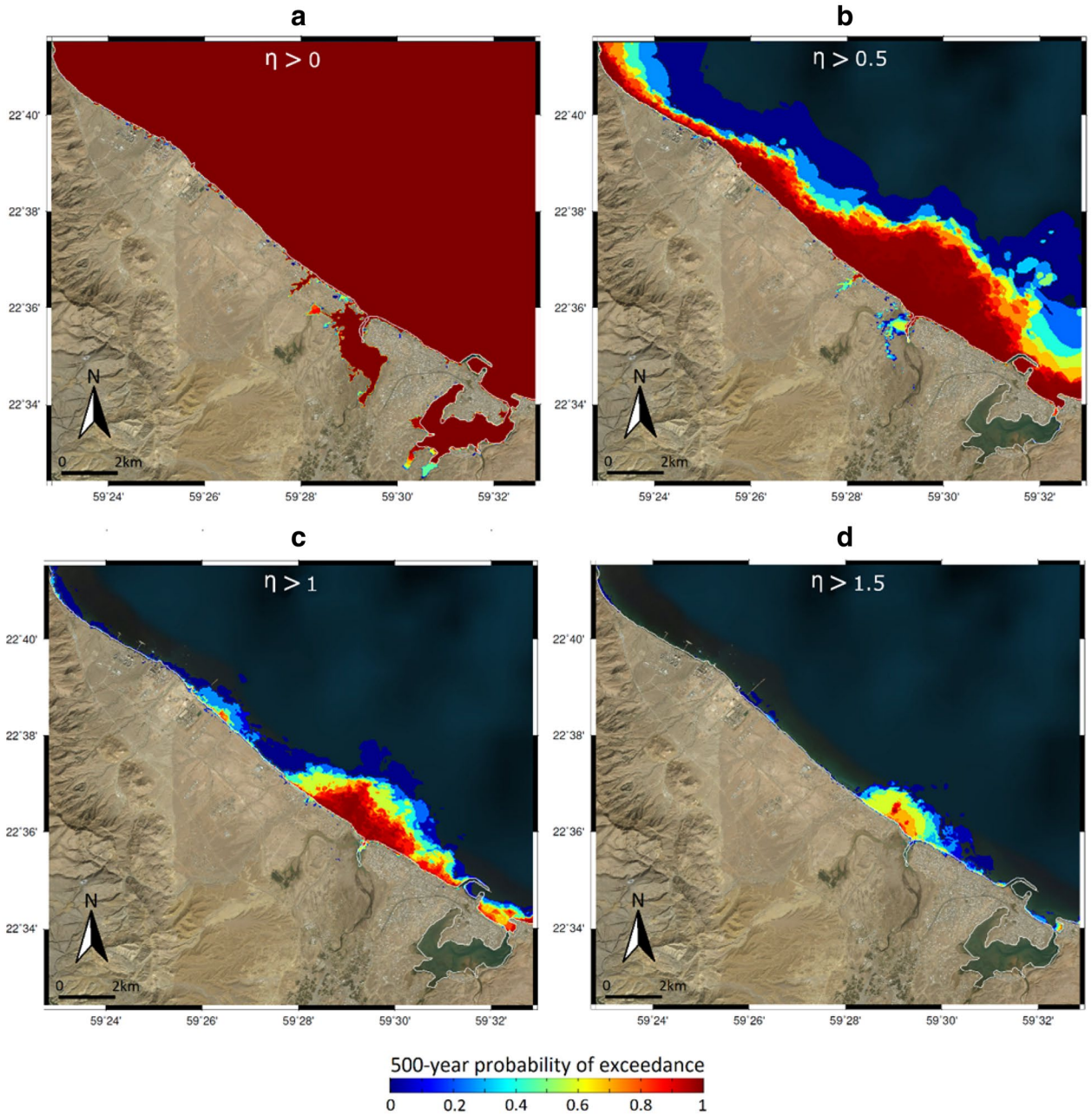

Fig. 7 Probability that the maximum wave height/flow depth **a** exceeds 0 m, **b** exceeds 0.5 m, **c** exceeds 1 m, and **d** exceeds 1.5 m along the coastal segment of Sur, Oman, for an exposure time of 500 years. η = wave height–flow depth threshold. The scale bar unit is the probability from 0 to 100% (0.8 = 80%)

locations (Fig. 7). Also, in 500-year average return period the likelihood of tsunami flood occurrence in Sur is up to 100% (Fig. 7c) and up to 80% with a flow depth of 1 m.

For both 100- and 500-year exposure times, it appears that the level of tsunami hazard varies in offshore Sur, being greatest close to the coastline where the tsunami shoaling is important.

When comparing the DTHA and PTHA results, it is evident that deterministic analysis leads to larger inundation areas at Sur, Oman. This is mainly because the DTHA considers the most credible worst-case ones occurring at once while PTHA takes the contribution

of all possible scenarios in MSZ with low probability of occurrence. The difference in the coastal flood area becomes smaller with larger return periods.

Conclusions

Tsunami hazard assessments along a coastal segment of Oman are evaluated using both deterministic and probabilistic approaches. Only tsunamis of earthquake origin generated in the Makran subduction zone are considered in this study as tsunamis generated by far-field tectonic sources cause very modest impact on this segment of the Omani coast. To perform a comprehensive tsunami hazard assessment, a benchmarked numerical model and a high-resolution coastal DEM combined with seismic source probability models is utilized. The results are presented for the costal site of Sur, Oman, and express the coastal impact and its likelihood of occurrence in 100- and 500-year average return times. The main findings are:

1. The tsunami hazard is significant along the coastal segment of Sur, Oman.
2. The maximum wave height from the worst-case tsunami scenario in the eastern MSZ reaches 2.5 m causing inundation of the low-lying coast of Sur.
3. In 100-year exposure time, the probability that a maximum wave amplitude exceeds 1 m varies from 50% up to 80%.
4. In 500-year average return period, the likelihood of tsunami flood occurrence in Sur is up to 100%.
5. DTHA leads to larger inundation at Sur coast than the PTHA.

These findings may enhance tsunami warning when integrated with earthquake parameters produced in real time of earthquake monitoring. This application can be improved by clarifying Makran tsunami sources, adding far-field and slide-induced tsunamis to the probabilistic assessment, and using improved digital elevation and tsunami-numerical models.

Authors' contributions

All authors contributed substantially to the preparation of this manuscript. All authors read and approved the final manuscript.

Author details

[1] Earthquake Monitoring Center, Sultan Qaboos University (SQU), Muscat, Oman. [2] Instituto Português do Mar e da Atmosfera, IPMA, Lisbon, Portugal. [3] Instituto Dom Luiz, IDL, University of Lisbon, Lisbon, Portugal. [4] Instituto Superior de Engenharia de Lisboa, ISEL, Instituto Politécnico de Lisboa, Lisbon, Portugal.

Acknowledgements

We thank Sultan Qaboos University (SQU) and the staff of the Earthquake Monitoring Center for supporting this project. We would like also to thank Christopher Jamed Denman from the Language Center at SQU for his assistance in editing and proofreading the manuscript. The authors wish to thank the Instituto Dom Luiz, IDL, and University of Lisbon, Portugal, for use of computing facilities. Thanks are also due to the two anonymous reviewers and the guest editor for their constructive and valuable scientific and editorial comments.

Competing interests

The authors declare that they have no competing interests.

Availability of data and materials

Not applicable.

Consent for publication

Not applicable.

Ethics approval and consent to participate

Not applicable.

Funding

Funding was provided by Sultan Qaboos University (Grant no. DVC/EMC).

Publisher's Note

Received: 26 April 2018 Accepted: 3 December 2018
Published online: 18 December 2018

References

Ambraseys NN, Melville CP (1982) A history of Persian earthquakes. Cambridge University Press, Cambridge, p 219

Baptista MA, Miranda JM, Omira R, Antuns C (2011) Potential inundation of Lisbon downtown by a 1755-like tsunami. Nat Hazards Earth Syst Sci 11:3319–3326

Bayer R, Chery J, Tatar M, Vernant P, Abbassi M, Masson F, Nilforousshan F, Doerflinger E, Regard V, Bellier O (2006) Active deformation in Zagros-Makran transition zone inferred from GPS measurements. Geophys J Int 165:373–381

Burbidge DR, Cummins PR, Mleczko R, Latief H, Mokhtari M (2009) A probabilistic tsunami hazard assessment of the Indian Ocean Nations: Geoscience Australia Professional Opinion No. 2009/11

Byrne DE, Sykes LR, Davis SM (1992) Great thrust earthquakes and aseismic slip along the plate boundary of the Makran subduction zone. J Geophys Res 97:449–478

Deif A, El Hussain I (2012) Seismic moment rate and earthquake mean recurrence interval in the major tectonic boundaries around Oman. J Geophys Eng 9:773–783. https://doi.org/10.1088/1742-2132/9/6/773

El-Hussain I, Omira R, Deif A, Al-Habsi Z, Al-Rawas G, Mohamad A, Al-Jabri K, Baptista MA (2016) Probabilistic tsunami hazard assessment along Oman coast from submarine earthquakes in the Makran subduction zone. Arab J Geosci 9(888):1–14. https://doi.org/10.1007/s12517-016-2687-0

El-Hussain I, Omira R, Al-Bloushi K, Deif A, Al-Habsi Z, Al-Rawas G, Mohamed AME, Al-Jabri K, Baptista MA (2017) Tsunami hazard assessment along Diba-Oman and Diba-Al-Emirates coasts. In: MATEC web of conferences, vol 120, p 06007, 71200. https://doi.org/10.1051/matecconf/201712006007

Geist EL, Lynett PJ (2014) Source processes for the probabilistic assessment of tsunami hazards. Oceanography 27(2):86–93

Geist EL, Parsons T (2006) Probabilistic analysis of tsunami hazards. Nat Hazards 37(3):277–314

Grezio A, Babeyko A, Baptista MA, Behrens J, Costa A, Davies G, Geist EL, Glimsdal S, González FI, Griffin J, Harbitz CB, LeVeque RJ, Lorito S, Omira R, Mueller C, Paris R, Parsons T, Polet J, Power W, Jacopo S, Mathilde B, Sørensen HK (2017) Probabilistic tsunami hazard analysis: multiple sources and global applications. Rev Geophys 55:1158–1198. https://doi.org/10.1002/2017RG000579

Gutenberg B, Richter CF (1954) Seismicity of the earth and associated phenomena. Hafner, New York

Harbitz CB, Glimsdal S, Bazin S, Zamora N, Løvholt F, Bungum H, Smebye H, Gauer P, Kjekstad O (2012) Tsunami hazard in the Caribbean: regional

exposure derived from credible worst case scenarios. Cont Shelf Res 38:1–23
Heidarzadeh M, Satake K (2017) A combined earthquake–landslide source model for the tsunami from the 27 November 1945 Mw 8.1 Makran earthquake. Bull Seismol Soc Am 107:1033–1040. https://doi.org/10.1785/0120160196
Heidarzadeh M, Pirooz MD, Zaker NH (2009) Modeling the near-field effects of the worst-case tsunami in the Makran subduction zone. Ocean Eng 36:368–376. https://doi.org/10.1016/j.oceaneng.2009.01.004
Hoffmann G, Rupprechter M, Al Balushi N, Grützner C, Reicherter K (2013) The impact of the 1945 Makran tsunami along the coastlines of the Arabian Sea (Northern Indian Ocean)—a review. Z Geomorphol Suppl Issue 57(supplement 4):257–277. https://doi.org/10.1127/0372-8854/2013/S-00134
Kakar DM, Naeem G, Usman A, Hasan H, Lodhi HA, Srinivasalu S, Andrade V, Rajendran CP, Beni AN, Hamzeh MA (2014) Elders recall an earlier tsunami on Indian Ocean shores. EOS Trans Am Geophys Union 95(51):485–486
Kakar DM, Naeem G, Usman A, Mengal A, Naderi Beni A, Afarin M, Ghaffari H, Fritz HM, Pahlevan F, Okal EA, Hamzeh M A, Ghasemzadeh J, Al-Balushi N S, Hoffmann G, Roepert A, Seshachalam S, Andrade V (2015) Remembering the 1945 Makran tsunami; interviews with survivors beside the Arabian Sea. UNESCO-IOC Brochure 2015-1, p 79. http://iotic.ioc-unesco.org/images/xplod/resources/material/1945Makrantsunami_2mb.pdf
Kukowski N, Schillhorn T, Flueh ER, Huhn K (2000) Newly identified strike-slip plate boundary in thenortheastern Arabian Sea. Geology 28:355–358
Liu PLF, Cho YS, Briggs MJ, Kanoglu U, Synolakis CE (1995) Runup of solitary waves on a circular island. J Fluid Mech 302:259–285
Lorito S, Tiberti MM, Basili R, Piatanesi A, Valensise G (2008) Earthquake-generated tsunamis in the Mediterranean Sea: scenarios of potential threats to southern Italy. J Geophys Res Solid Earth. https://doi.org/10.1029/2007JB004943
Løvholt F, Bungum H, Harbitz CB, Glimsdal S, Lindholm CD, Pedersen G (2006) Earthquake relatedtsunami hazard along the western coast of Thailand. Nat Hazard Earth Syst 6:979–997
Masson F, Anvari M, Djamour Y, Walpersdorf A, Tavakoli F, Daignieres M, Nankali H, Van Gorp S (2007) Large-scale velocity field and strain tensor in Iran inferred from GPS measurements: new insight for the present-day deformation pattern within NE Iran. Geophys J Int 170:436–440
McCall GJH (2002) A summary of the geology of the Iranian Makran. In: Clift PD, Kroon D, Gaedicke C, Craig J (eds) The tectonic and climatic evolution of the Arabian Sea Region, vol 195. Geological Society of London, London, pp 147–204 **(Special Publications)**
Minshull TA, White RS, Barton PJ, Collier JS (1992) Deformation at plate boundaries around the Gulf of Oman. Mar Geol 104(1–4):265–277
Miranda JM, Luis J, Reis C, Omira R, Baptista MA (2014) Validation of NSWING, a multi-core finite difference code for tsunami propagation and run-up. In: American Geophysical Union (AGU) fall meeting, San Francisco. Paper number: S21A-4390, Session number and Title: S21A, Natural Hazards
Molnar P (1979) Earthquake recurrence intervals and plate tectonics. Bull Seismol Soc Am 69:115–133
Mori N, Takahashi T, Yasuda T, Yanagisawa H (2011) Survey of 2011 Tohoku earthquake tsunami inundation and run-up. Geophys Res Lett. https://doi.org/10.1029/2011gl049210
Musson RMW (2009) Subduction in the western Makran: the historian's contribution. J GeolSoc 166:387–391
Okada Y (1985) Surface deformation due to shear and tensile faults in a half-space. Bull Seismol Soc Am 75(4):1135–1154
Okal EA, Synolakis CE (2008) Far-field tsunami hazard from mega-thrust earthquakes in the Indian Ocean. Geophys J Int 172:995–1015. https://doi.org/10.1111/j.1365-246x.2007.03674.x
Okal EA, Fritz HM, Raad PE, Synolakis C, Al-Shijbi Y, Al-Saifi M (2006) Oman field survey after the December 2004 Indian Ocean Tsunami. Earthquake Spectra 22(S3):203–218
Omira R, Baptista MA et al (2013) Performance of coastal sea-defense infrastructure at El Jadida (Morocco) against tsunami threat: lesson learned from the Japanese 11th March 2011, tsunami. Nat Hazards Earth Syst Sci 13:1–16
Omira R, Baptista MA, Matias L (2015) Probabilistic tsunami hazard in the Northeast Atlantic from near-and far-field tectonic sources. Pure Appl Geophys 172(3–4):901–920
Omira R, Matias L, Baptista MA (2016a) Developing an event-tree probabilistic tsunami inundation model for NE Atlantic coasts: application to a case study. Pure Appl Geophys 173(12):3775–3794
Omira R, Baptista MA, Lisboa F (2016b) Tsunami characteristics along the Peru–Chile trench: analysis of the 2015 Mw 8. 3 Illapel, the 2014 Mw 8. 2 Iquique and the 2010 Mw 8. 8 Maule tsunamis in the near-field. Pure Appl Geophys 173(4):1063–1077
Page WD, Alt JN, Cluff LS, Plafker G (1979) Evidence for the recurrence of large-magnitude earthquakes along the Makran coast of Iran and Pakistan. Tectonophysics 52(1):533–547
Pararas-Carayannis G (2006) The potential of tsunami generation along the Makran subduction zone in the Northern Arabian sea. Case study: the earthquake tsunami and tsunami of November 28, 1945. Sci Tsunami Hazards 24:358
Quittmeyer RC, Jacob KH (1979) Historical and modern seismicity of Pakistan, Afghanistan, northwestern India, and southeastern Iran. Bull Seismol Soc Am 69:773–823
Rashidi A, Shomali ZH, Keshavarz Farajkhah N (2018) Tsunami simulations in the western Makran using hypothetical heterogeneous source models from world's great earthquakes. Pure Appl Geophys 175:1325–1340. https://doi.org/10.1007/s00024-018-1842-9
Rastgoftar E, Soltanpour M (2016) Study and numerical modeling of 1945 Makran tsunami due to a probable submarine landslide. Nat Hazards 83:929–945. https://doi.org/10.1007/s11069-016-2356-3
Regard V, Hatzfeld D, Molinaro M, Aubourg C, Bayer R, Bellier O, Yamini-Fard F, Peyret M, Abbassi M (2010) The transition between Makran subduction and the Zagros collision: recent advances in its structure and active deformation. In: Leturmy P, Robin C (eds) Tectonic and stratigraphic evolution of Zagros and Makran during the Mesozoic-Cenozoi, vol 330. Geological Society of London, London, pp 43–64 **(Special Publication)**
Smith GL, McNeill LC, Wang K, He J, Henstock TJ (2013) Thermal structure and megathrust seismogenic potential of the Makran subduction zone. Geophys Res Lett 40:1528–1533. https://doi.org/10.1002/grl.50374
Tinti S, Armigliato A (2003) The use of scenarios to evaluate the tsunami impact in southern Italy. Mar Geol 199(3):221–243
Tinti S, Armigliato A, Pagnoni G, Zaniboni F (2005) Scenarios of giant tsunamis of tectonic origin in the Mediterranean. ISET J Earthquake Technol 42(4):171–188
Vernant Ph, Nilforoushan F, Hatzfeld D, Abassi MR, Vigny C, Masson F, Nankali H, Martinod J, Ashtiani A, Bayer R, Tavakoli F, Chery J (2004) Present-day crustal deformation and plate kinematics in Middle East constrained by GPS measurements in Iran and northern Oman. Geophys J Int 157:381–398
Wessel P, Smith WH, Scharroo R, Luis J, Wobbe F (2013) Generic mapping tools: improved version released. EOS Trans Am Geophys Union 94(45):409–410
Zarifi Z (2006) Unusual subduction zones: case studies in Colombia and Iran. University ofBergen, Norway